Chapter 3

Second derivative of Gaussian based matched filter approach for retinal blood vessels segmentation

3.1 Introduction

The automated retinal blood vessel segmentation is a prominent task for computer aided diagnosis of retinal pathologies such as glaucoma [139], hypertension [140], diabetes [2, 44], obesity [12], etc. Vessels structure are similar to the cluster of lines so retinal blood vessel segmentation is a line detection problem. After a deep literature survey it is found that various methods have been proposed for retinal blood vessel segmentation. According to author M. M. Fraz *et al.* [6] the retinal blood vessel segmentation approaches are mainly classified into seven categories, namely, the intensity based pattern recognition techniques, mathematical morphology based, vessel tracking based, model based, parallel hardware based, multi-scale based techniques and matched filter based approach. These seven categories are briefly discussed in Chapter 2.

Here we start the discussion about the matched filter based approach because the proposed approach is based on that due to their simplicity and effectiveness. The matched filter based approach detect the retinal blood vessel by applying matched filter and thresh-

olding on the original input retinal image [12]. To design a matched filter kernel, three points are important which include limited curvature of vessels which may be approximated by piecewise linear segments, the width of the vessels which gradually decreases when one move away from the optical disk of the retinal image, and cross-sectional intensity profile of retinal blood vessels which have approximate Gaussian shape. Due to the consideration of the cross-sectional intensity profile of retinal blood vessels which is approximated by Gaussian shape, the sequence of Gaussian shaped filters are required for the detection of whole retinal blood vessels. Generally the matched filter provide a strong response for both vessels as well as non-vessel edges. That's why there will be many false detections that may exist in the image after applying thresholding. The matched filter based approaches use the prior knowledge about the Gaussian shaped cross-section profile of the retinal blood vessel but cannot be used for other information such as about the symmetry of the Gaussian shape with respect to their peak position and zero-crossing. If these properties are used in proper way, the accuracy of retinal blood vessel segmentation can be improved.

To this end, a novel method, namely second order derivative of Gaussian based matching filter (SDOG-MF) approach for retinal blood vessel segmentation have been proposed. This approach considers two things namely the symmetry of the Gaussian shape with respect to their peak position, and information about zero-crossing. The second order derivative of Gaussian provide a strong response around their peak positions and zero-crossings are useful to identify the positions where the second order derivatives become zero, and these positions correspond to double edge positions. In this approach, we investigate and propose a fast and efficient retinal blood vessel segmentation method by applying the SDOG matched filter. The proposed method concentrates towards the segmentation of thin as well as thick retinal blood vessels.

3.2 Background

The proposed modified retinal image segmentation approach comes in the category of matched filter based approach. There are various matched filters based retinal blood ves-

sel segmentation approaches which exist in literature. In the previous section, the basic concepts of matched filter are discussed. In this section, our objective is to present, how much work has been done previously. First time author Chaudhuri *et al.* [12] proposed an approach based on two-dimensional matched filters for the retinal blood vessels extraction by using some assumptions such as the intensity profile have been approximated by a Gaussian function, the vessels have been approximated by piecewise linear segments and the width of the vessels are constant. Finally, for the detection of blood vessel the matched filter was applied in several orientations. The author T. William *et al.* [141] designed a steerable filter, which was a filter with arbitrary orientations and had been organized from the linear combinations of normal filters. Hoover *et al.* [2] proposed an approach for retinal blood vessels segmentation by combining the local and regional-based properties and used the threshold probing technique on a matched filter response image. Luo Gang *et al.* [142] used an amplitude modified second order Gaussian filter for the detection of retinal blood vessel and showed that the vessel width provide the size of blood vessels as well as are useful for optimization of matched filter that improve the rate of efficiency of vessel detection. Xiaoyi *et al.* [44] proposed an adaptive local thresholding framework based on verification-based multi-threshold probing scheme which is also used for retinal vessel detection. Al-Rawi *et al.* [13] proposed an improved matched filter for retinal blood vessel detection and author Fielder *et al.* [143] proposed an automatic blood vessels extraction approach for low quality and noisy retinal images. Chang Yao et al [71] used a two-dimensional Gaussian matched filter for enhancement of retinal blood vessel and then a simplified pulse coupled neural network [144] for the vessel segmentation by firing neighborhood neurons. The author Cinsdikici *et al.* [45] proposed a hybrid model of matched filter and ANT colony optimization [145] for retinal blood vessel extraction. Zhang *et al.* [47] proposed matched filter with first-order derivative of Gaussian which is the generalized and extended form of the classical Gaussian-shaped matched filter proposed by Chaudhuri *et al.* [12].

3.3 Methods and model

The first matched filter was proposed by author Chaudhuri *et al.* [12] to detect the retinal blood vessels by using zero-mean Gaussian function based matched filter, which is defined as

$$f(x,y) = -\exp^{-((x^2+y^2)/2\sigma^2)} \tag{3.1}$$

Where σ is variance which is used to increase the intensity profile. In case of retina, it is assumed that the direction of blood vessels to be aligned along the y-axis of the optical disk of the fundus image and L is the length of the segment for which the vessel have a fixed orientation. Then two dimensional matched filter kernels are designed by author Chaudhuri *et al.* [12] using a zero-mean Gaussian-shaped function which is defined as

$$f(x,y) = -\exp^{(-x^2/2\sigma^2)} \quad for \ \ |y| \leq L/2 \tag{3.2}$$

Where x is the perpendicular distance between point (x,y) and straight line passing through the center of retinal blood vessel. The zero-mean Gaussian-shaped matched filter makes it popular for retinal blood vessel detection but their exists a well-known problem that it detects both the vessels and non-vessels edges. The author Zhang *et al.* [47] proposed an extension and generalization of the zero-mean Gaussian-shaped matched filter known as matched filter with first-order derivative of Gaussian by considering the cross section of a vessel is a symmetric Gaussian function, and use a combination of two filters, the zero-mean Gaussian filter and the first-order derivative of the Gaussian filter, to detect the retinal blood vessels. As previously discussed the zero-mean Gaussian matched filter has strong responses for both the vessels and non vessels of retinal image. So it is difficult to bifurcate these two structure of the retinal image. Based on these facts the SDOG-MF based segmentation approach is proposed by Singh N P *et al.* [204] . The second derivative of Gaussian matched function is defined as

$$f(x,y) = -\frac{(x-\sigma)(x+\sigma)}{\sqrt{2\pi}\sigma^5}\exp^{(-x^2/2\sigma^2)} \tag{3.3}$$

where $|y| \leq L/2$.

This approach considers the symmetry of the Gaussian shape with respect to their peak position and zero-crossings. The second order derivative of Gaussian (SDOG) provides a strong response around their peak position and zero-crossing is useful to identify the position where the second order derivatives become zero, and these positions correspond to double edge positions. Our proposed approach is the combination of SDOG matched filter, entropy based optimal thresholding, vessel length filtering and removing outliers artifacts by using the concept of masking.

Generally, the blood vessels have low contrast with respect to their background so SDOG matched filter is used to enhance the retina image and generate a matched filter response (MFR) image, in which the entropy based optimal thresholding scheme [12] have been applied to differentiate the retinal blood vessels from their background. After that length filtering criterion [12] is applied to remove the misclassified pixels, and finally the outliers artifacts are removed by applying mask, generated by using particular retinal image which contains the boundary of retinal image. The model of the proposed work is shown in Figure 3.1.

The author Xu *et al.* [51] state that the width of thin blood vessel segments varies from 3 to 5 and a thick blood vessel segment varies from 9 to 12 pixels. The author Azegrouz *et al.* [146] state that the tortuosity of human retinal blood vessels is an indicator of many diseases, which depends on the width of retinal blood vessels. The tortuosity of thin retinal blood vessels is an indicator of the initial stage of diseases whereas a the tortuosity of thick blood vessels indicates the next stage of the diseases. This gives an idea to setup the parameters of SDOG matched filter. Hence, we consider the length of vessel segment $L = 5$ that cover thin as well as thick blood vessels. The author Azegrouz *et al.* [146] also state that in general the width of retinal blood vessels are 10 pixels but in presence of retinal pathology it may increase. Therefore to evaluate the performance of proposed approach use the kernel size 10×10 and angular revolution 30^o. According to these assumption, to cover all possible orientations, six different kernels are required in proposed approach.

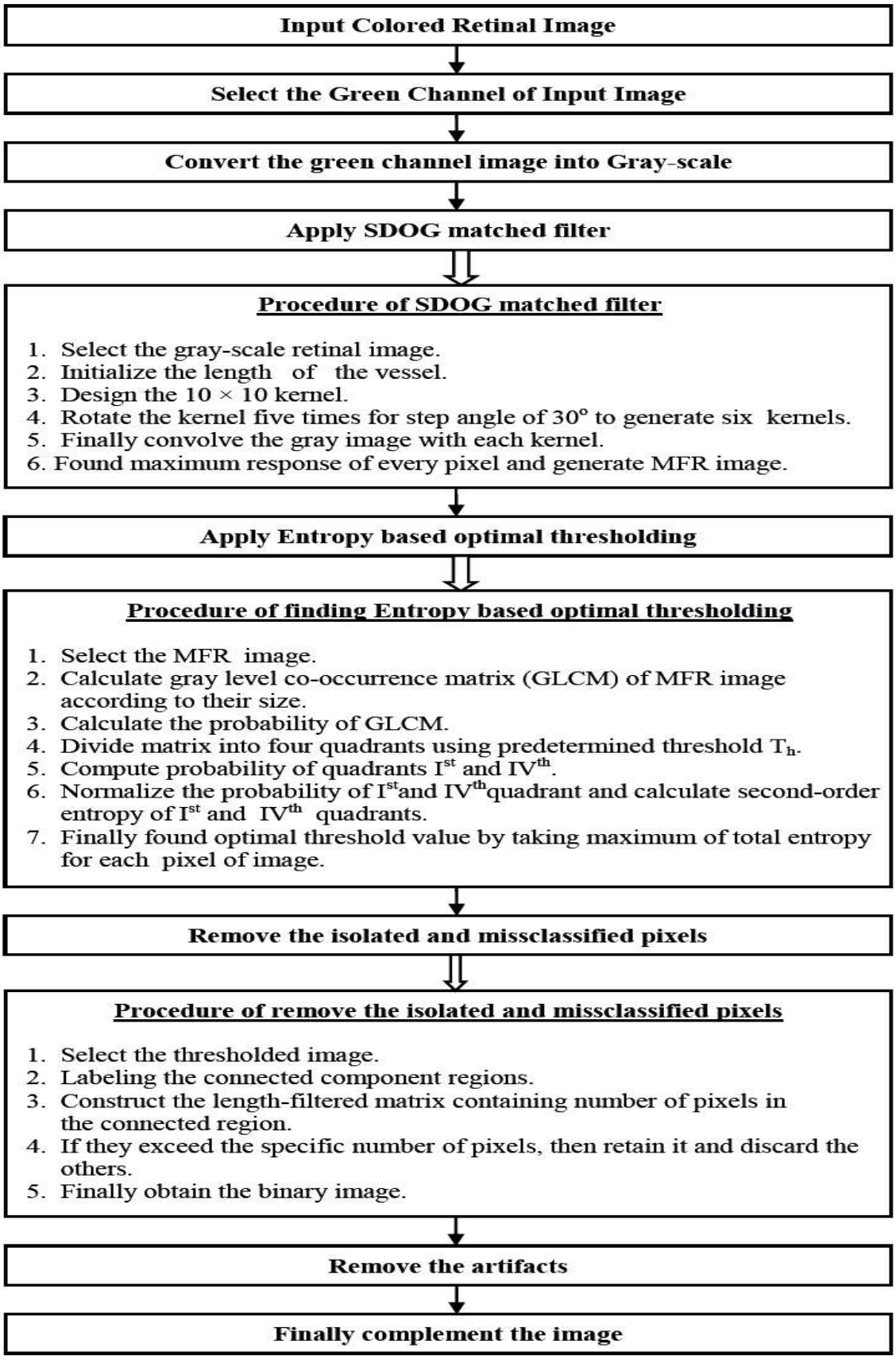

Figure 3.1: Proposed Model

To truncate the trail of Gaussian curve, $x = \pm 1\sigma$ have been used. Finally, the kernel is applied by convolving to retinal image and only the maximum response was retained at each pixel. The above chosen parameters are based on exhaustive experimentation on the chosen datasets and are associated to better performance in comparison to all other previous implementations. For example, the proposed SDOG matched filter response image, according to these assumptions are shown in Figure 3.2(d) and Figure 3.3(d) for images taken from DRIVE data set and STARE data set respectively.

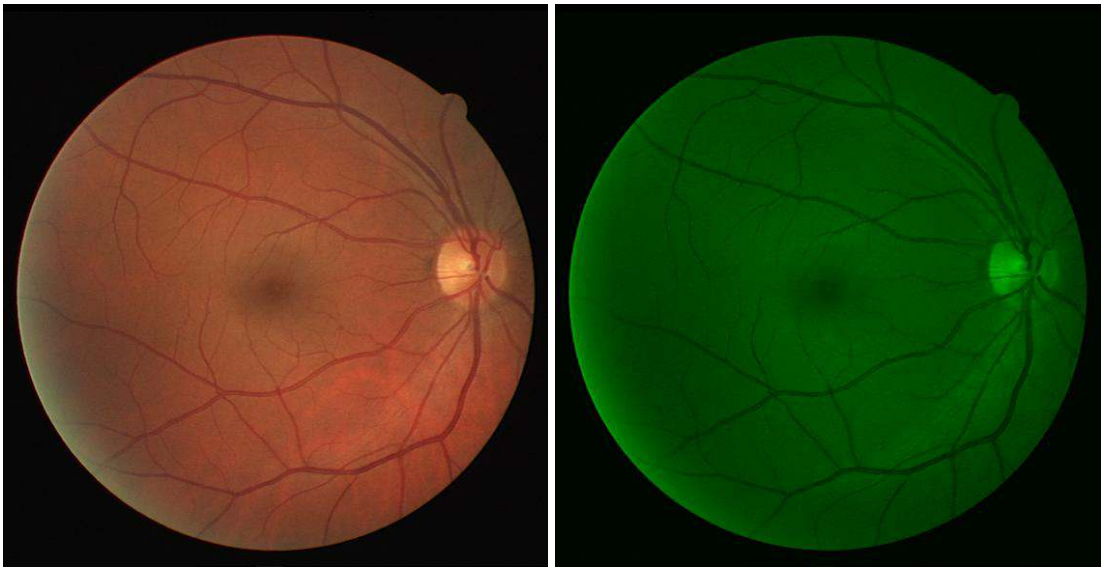

(a) (b)

(c) (d)

Figure 3.2: For image taken from DRIVE data set (a) Original image (b) Selected green channel of input image (c) Gray-scale image (d) Proposed SDOG Matched Filter [204] Response image

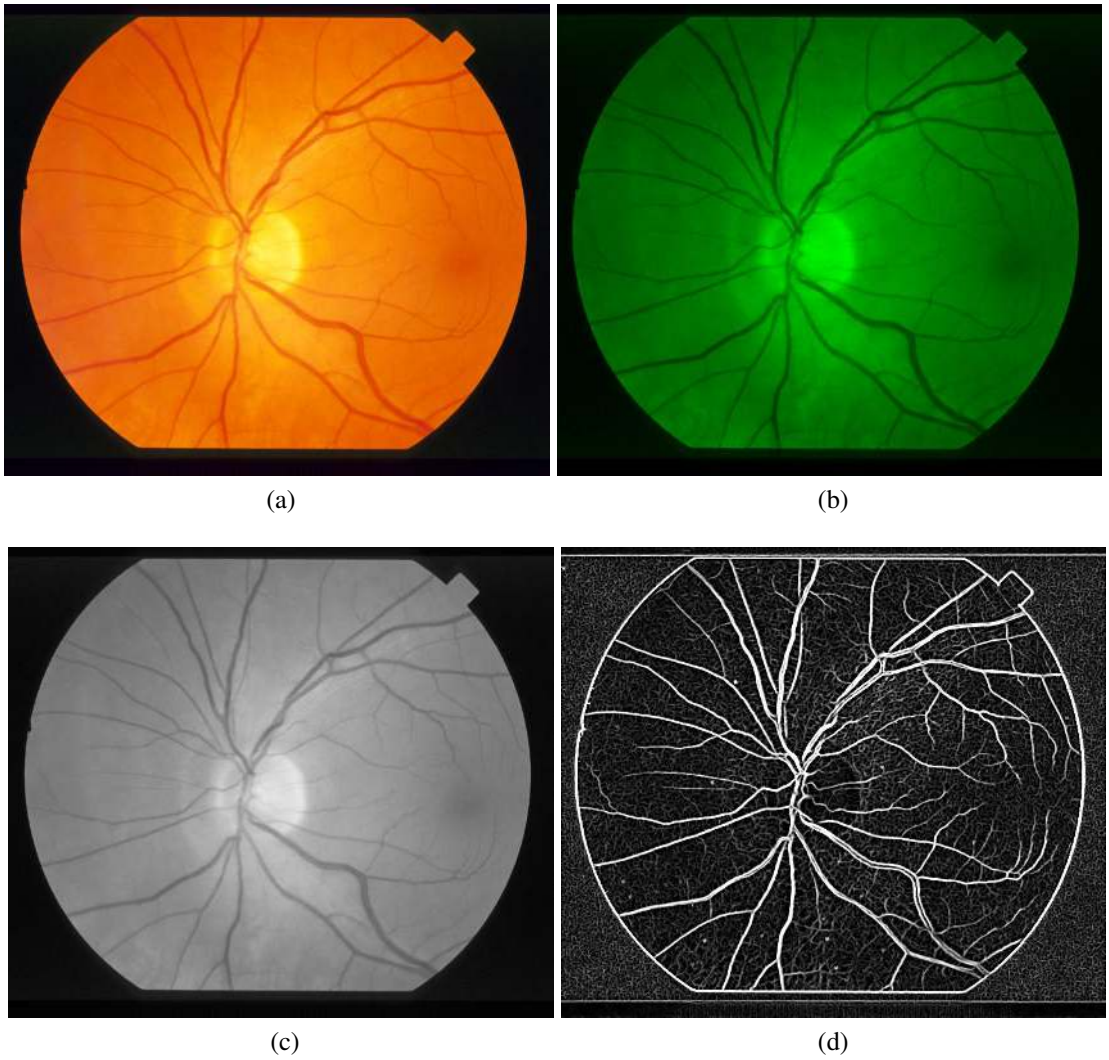

Figure 3.3: For image taken from STARE data set (a) Original image (b) Selected green channel of input image (c) Gray-scale image (d) Proposed SDOG Matched Filter [204] Response image

3.3.1 Vessels Extraction and Local Thresholding

An effective thresholding scheme is required for extraction of blood vessels, after finding enhanced blood vessel image by SDOG matched filter response. According to the authors Chaudhuri *et al.* [12] and M. M. Fraz *et al.* [6] the entropy based optimal thresholding perform better with respect to other thresholding techniques used by authors Al-Rawi *et al.* [13], Xiaoyi and Mojon [44], Cinsdikici *et al.* [45], and Amin and Yan [46]. Therefore in proposed approach, the entropy based optimal thresholding is used for extraction of blood vessels. The Gray Level Co-occurrence Matrix (GLCM) is required to compute

the optimal threshold value by taking the spatial distribution of gray levels and embedded with co-occurrence matrix because the intensity of image pixels are not independent to other pixels. The GLCM is important for finding the threshold value because it contains the information of frequency distribution of gray level and edge information. Here, we consider the size of GLCM matrix to be $P \times P$ of gray level image having spatial dimension $R \times C$ with range of gray levels [0,1,.....,P-1]. The GLCM matrix is represented by $T = [t_{ij}]_{P\times P}$. The element of matrix for each image pixel at specific coordinate (r, c) with its gray level is specified by $f(r, c)$ by considering its nearest neighboring pixels. The co-occurrence matrix is designed by comparing gray level changes of $f(r, c)$ to its corresponding gray levels by considering horizontally right and vertically lower transitions. Thus the elements t_{ij} of the co-occurrence matrix T is defined by Eq^n-3.4 and Eq^n-3.5.

$$t_{ij} = \sum_{r=1}^{R}\sum_{c=1}^{C} \delta \tag{3.4}$$

where

$$\delta = 1 \text{ if } \begin{cases} f(r,c) = i \quad \text{and} \quad f(r,c+1) = j, \\ \qquad\qquad \text{or} \\ f(r,c) = i \quad \text{and} \quad f(r+1,c) = j. \end{cases} \tag{3.5}$$

$$\delta = 0 \qquad \text{otherwise}$$

For gray levels i and j the co-occurrence probability (p_{ij}) calculated by using Eq^n-3.6

$$p_{ij} = \frac{t_{ij}}{\sum_i \sum_j t_{ij}} \tag{3.6}$$

where t_{ij} is the co-occurrence matrix define in Eq^n-3.5. Due to the gray level variations between enhanced retinal blood vessels and their background, the co-occurrence matrix is divided in four quadrants, namely I, II, III and IV quadrant having threshold (T_h) value within range $0 \leq T_h \leq P-1$ as shown in Figure 3.4. Further these four quadrants are grouped into two classes. The class one contains quadrant I^{st} and IV^{th} that is known as local quadrant and second class contains quadrant II^{nd} and III^{rd} that is known as joint

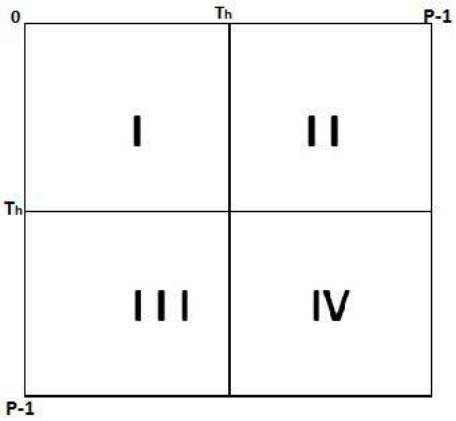

Figure 3.4: Division of Co-occurrence matrix

quadrant. For calculating local entropy thresholding only local quadrant is considered, because it contains the gray level transition that arises within the blood vessel or the background. The probability of quadrant I^{st} and IV^{th} is calculated by using Eq^n-3.7 and Eq^n-3.8 respectively.

$$P_I = \sum_{i=0}^{T_h} \sum_{j=0}^{T_h} p_{ij} \tag{3.7}$$

$$P_{IV} = \sum_{i=T_h+1}^{P-1} \sum_{j=T_h+1}^{P-1} p_{ij} \tag{3.8}$$

$$P_{ij}^{I} = \frac{t_{ij}}{\sum_{i=0}^{T_h} \sum_{j=0}^{T_h} t_{ij}} \tag{3.9}$$

for $0 \leq i \leq T_h$ and $0 \leq j \leq T_h$

similarly

$$P_{ij}^{IV} = \frac{t_{ij}}{\sum_{i=T_h+1}^{P-1} \sum_{j=T_h+1}^{P-1} t_{ij}} \tag{3.10}$$

for $T_h + 1 \leq i \leq L - 1$ and $T_h + 1 \leq j \leq L - 1$

After that normalizing the probabilities of each quadrant in such a way that the summation of the probabilities of each quadrant equals one and normalization of the quadrant probabilities of I^{st} and IV^{th} quadrants (P_{ij}^{I} and P_{ij}^{IV}) are evaluated by using Eq^n-3.9 and

Eq^n-3.10. In next step, we calculate the second-order entropy of the blood vessels (i.e.I^{st} quadrant), denoted by $H_I(T_h)$ and defined by Eq^n-3.11. Similarly the second-order entropy of the background is denoted by $H_{IV}(T_h)$ and defined by Eq^n-3.12.

$$H_I(T_h) = -\frac{1}{2}\sum_{i=0}^{T_h}\sum_{j=0}^{T_h} P_{ij}^I \log_2 P_{ij}^I \tag{3.11}$$

$$H_{IV}(T_h) = -\frac{1}{2}\sum_{i=T_h+1}^{P-1}\sum_{j=T_h+1}^{P-1} P_{ij}^{IV} \log_2 P_{ij}^{IV} \tag{3.12}$$

The total second-order local transition entropy $H_{Total}(T_h)$ is calculated by adding $H_I(T_h)$ and $H_{IV}(T_h)$. Finally, the optimal local threshold denoted by T_{opt}, is defined by the gray level corresponding to maximum of $H_{Total}(T_h)$. The optimal threshold is able to classify the retinal blood vessels from their backgrounds which is shown in Figure 3.5(a) for DRIVE image and Figure 3.6(a) for STARE image.

3.3.2 Length filtering and removing outer artifacts

In Figure 3.5(a) and Figure 3.6(a) there exists some isolated and misclassified pixels, and they are removed by applying length filtering by using eight-connected neighborhood pixel label propagations to find a retinal blood vessels structure without any isolated and misclassified pixels, as shown in Figure 3.5(b) and Figure 3.6(b). It may be possible that some artifacts outside the region of interest may be included in retinal boundary. Hence, for removing these artifacts, masking is applied by using the mask generated by particular retinal image, as shown in Figure 3.5(c) and Figure 3.6(c). Finally, compliment of the segmented image (shown in Figure 3.5(d) and Figure 3.6(d)) are generated for evaluating the sensitivity, specificity and accuracy with respect to ground truth image given in DRIVE and STARE databases respectively.

3.4 Results and discussions

The proposed SDOG-MF method have been implemented on publicly available retinal fundus image databases, the DRIVE database [137] and the STARE database [2]. To

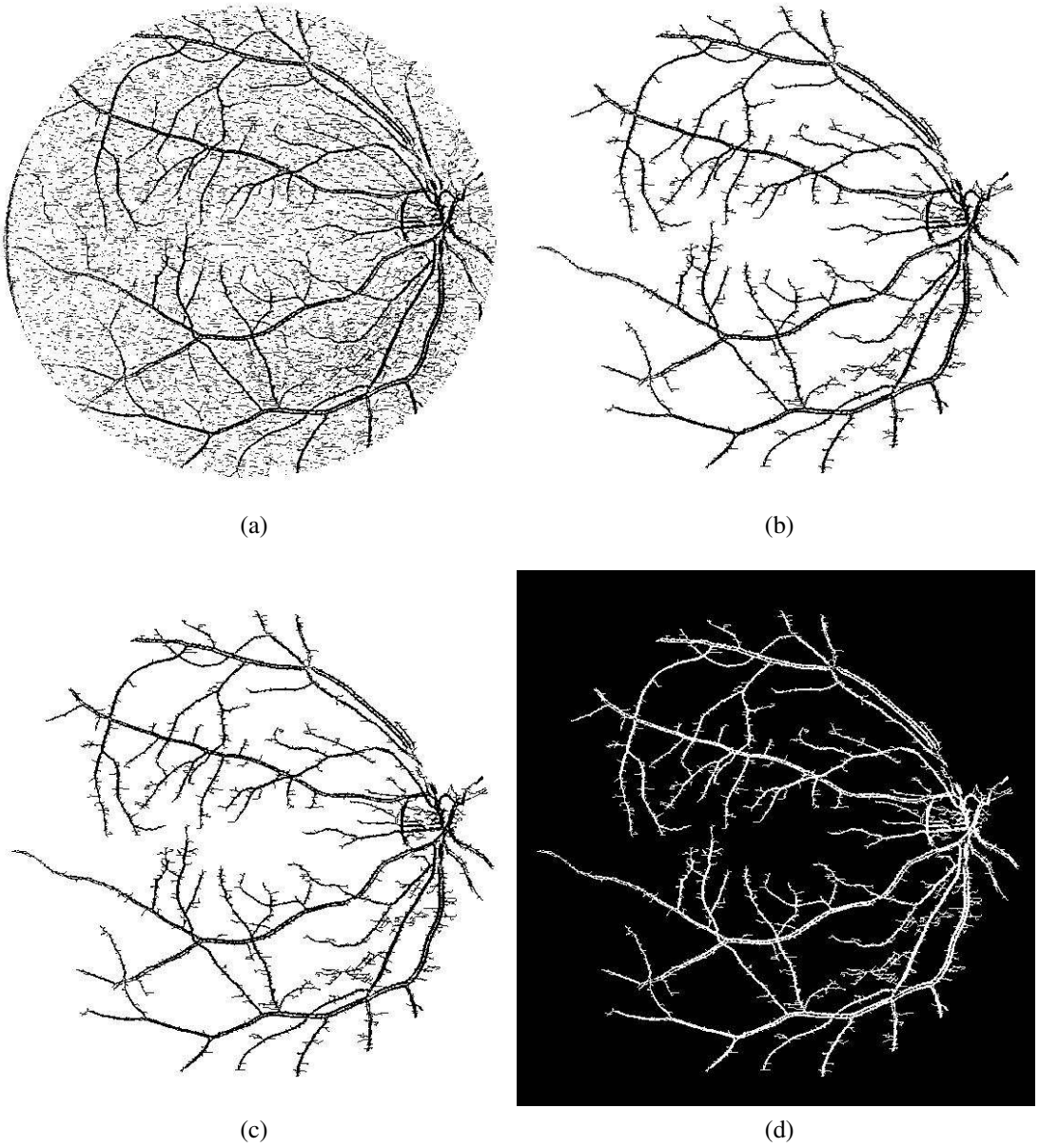

(a) (b)

(c) (d)

Figure 3.5: Details of image taken from DRIVE data set (a) classified blood vessels from their backgrounds (b) blood vessel without isolated and misclassified pixels (c) after removing outer artifacts (d) complimented segmented image for comparison with the existing Ground Truth Image

evaluate the performance of proposed approach, the color retinal image and respective ground truth image have been taken from DRIVE database as well as from STARE database. To compare the performance of different retinal vessel segmentation algorithms, we evaluated the accuracy, true positive rate (TPR), and the false positive rate (FPR). These quantitative performance measures are widely used and defined in literature [2, 44, 12, 26, 27, 66, 48, 56]. The accuracy of the segmentation algorithms is defined

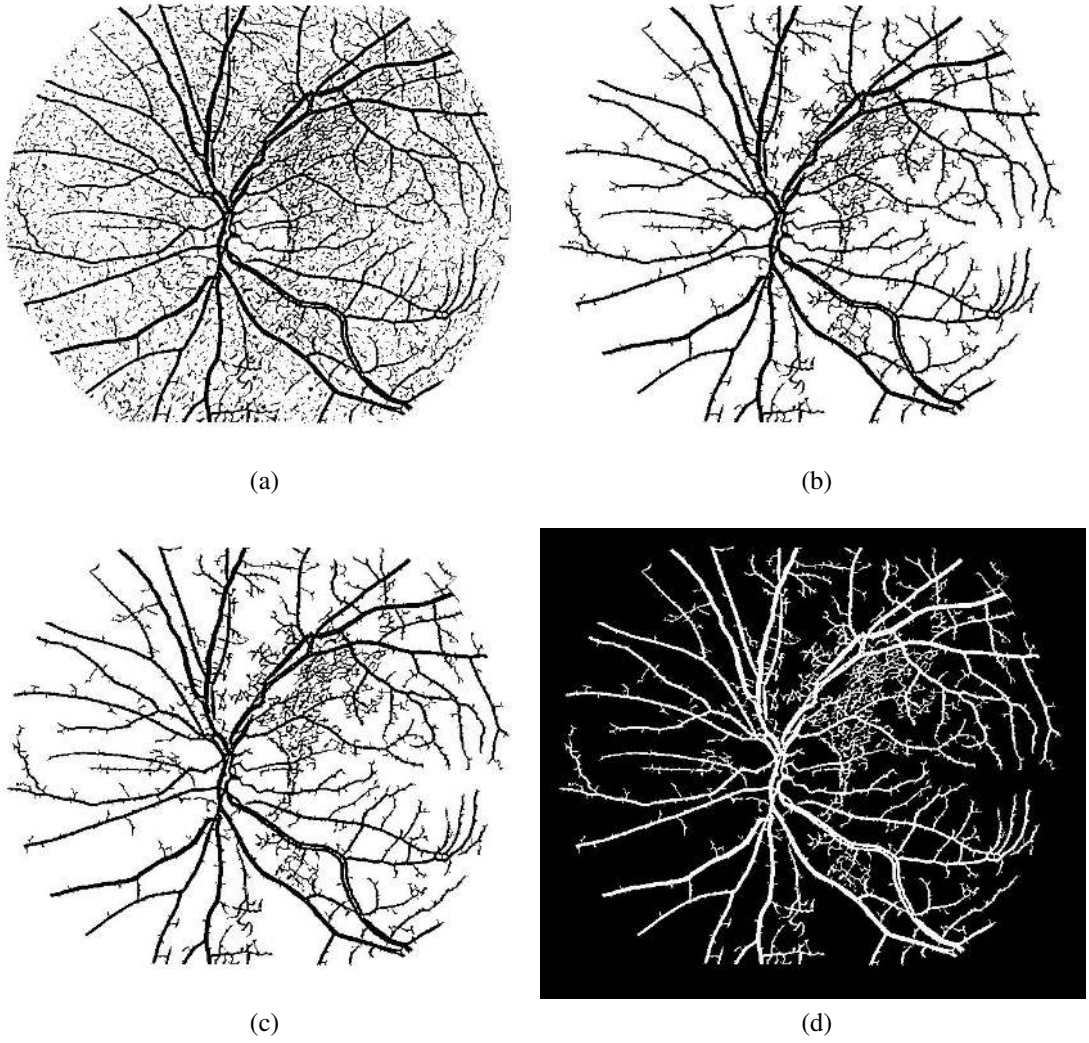

(a) (b)

(c) (d)

Figure 3.6: Details of image taken from STARE data set (a) classified blood vessels from their backgrounds (b) blood vessel without isolated and misclassified pixels (c) after removing outer artifacts (d) complimented segmented image for comparison with the existing Ground Truth Image

as the ratio of total correctly classified pixels with total number of pixels in the selected image. The TPR is the ratio of total correctly classified vessel pixels with total number of vessel pixels in the respective ground truth image and similarly the FPR is the ratio of total correctly classified non-vessel pixels with total number of non-vessel pixels in the respective ground truth image. The proposed vessels segmentation approach have been implemented on Matlab R2013a on a PC having AMD E-450 APU, Radeon with 1.65 GHz processor having 2 GB RAM. The average execution time of entire process for 40 images of DRIVE database and 20 images of STARE database took about 5.20 and 2.4 minutes respectively.

The comparative analysis of proposed vessel segmentation approach on the DRIVE database is presented in Table 3.1 and graphical representation of comparative performances are also shown in Figure 3.7, Figure 3.8, and Figure 3.9. All 20 original retinal images and respective ground truth images segmented by first human observer in the test set of DRIVE database were used to evaluate the performance of our proposed approach. The performance measures of retinal blood vessel segmentation methods proposed by [13], [30], [66] , [45], [62], [53], [46], and [68] were obtained from their original published papers. The authors Jiang *et al.* [44] and Zana *et al.* [55] proposed their segmentation approach in year 2003 and 2001, on that time the DRIVE database was not established. Hence the performance of their approaches were evaluated by Staal *et al.* [26] and Niemeijer *et al.* [27] respectively. The performance of vessel segmentation approach proposed by Frangi *et al.* [147], Perez *et al.* [67], Espona *et al.* [35], Palomera-Perez *et al.* [64],Martinez-Perez *et al.* [65], and Chaudhuri *et al.* [12] have been taken from survey paper published by Fraz *et al.*[6]. All retinal blood vessels segmentation approaches used for comparative analysis, are belongs to different categories as mentioned in Table 2.1 and Table 2.2 for DRIVE and STARE database respectively of Chapter 2. Whereas all the authors used the same database, so for comparative analysis of proposed approach we use their results. The overall TPR and accuracy measures of our proposed SDOG-MF approach for DRIVE database are better than the various existing approaches and overall FPR is inferior to some other existing approaches as mentioned in Table 3.1 and the graphical representation of TPR, FPR, and Accuracy are given in Figure 3.7, Figure 3.8, and Figure 3.9 respectively.

Table 3.1: Comparison of Vessel segmentation results on the DRIVE database

Author's name	**TPR**	**FPR**	**Accuracy**
Human observer	0.7761	0.0275	0.9473
Chaudhuri *et al.* [12]	0.6168	0.0259	0.9284
Zana *et al.* [55]	-	-	0.9377
Garg *et al.* [30]	-	-	0.9361
Perfetti *et al.* [62]	-	-	0.9261
Cinsdikici *et al.* [45]	-	-	0.9293
Al-Rawi *et al.* [13]	-	-	0.9510
Amin *et al.* [46]	-	-	0.9200
Anzalone *et al.* [68]	-	-	0.9419
Frangi *et al.* [147]	0.6565	0.0495	0.9270
Martinez-Perez *et al.* [65]	0.6389	-	0.9181
Jiang *et al.* [44]	0.6363	0.0338	0.9212
Perez *et al.* [67]	0.6600	0.0388	0.9220
Espona *et al.* [35]	0.6634	0.0318	0.9316
Palomera-Perez *et al.* [64]	0.6400	0.0330	0.9250
Zhang *et al.* [47]	0.7120	0.0276	0.9382
Marin *et al.* [53]	0.7067	0.0199	0.9452
Proposed Approach (SDOG-MF)	**0.6901**	**0.0354**	**0.9645**

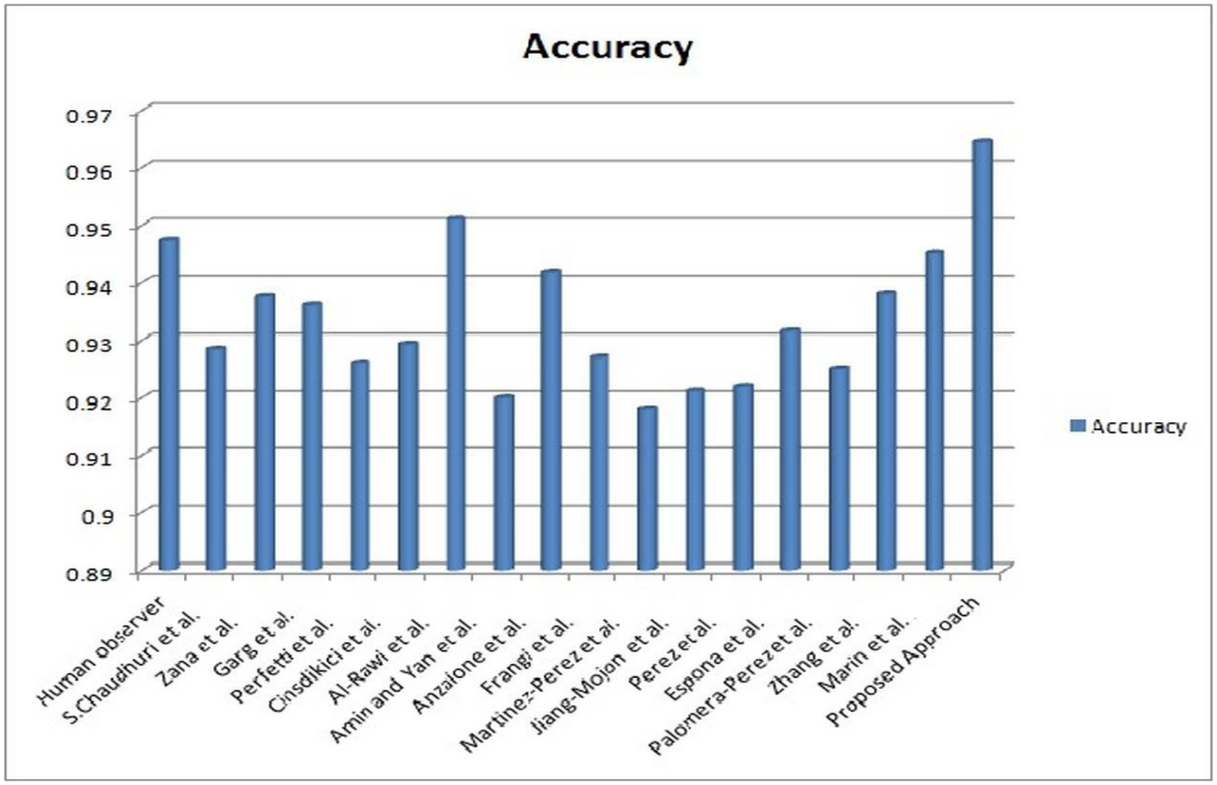

(a)

Figure 3.7: Comparison of Accuracy for DRIVE database.

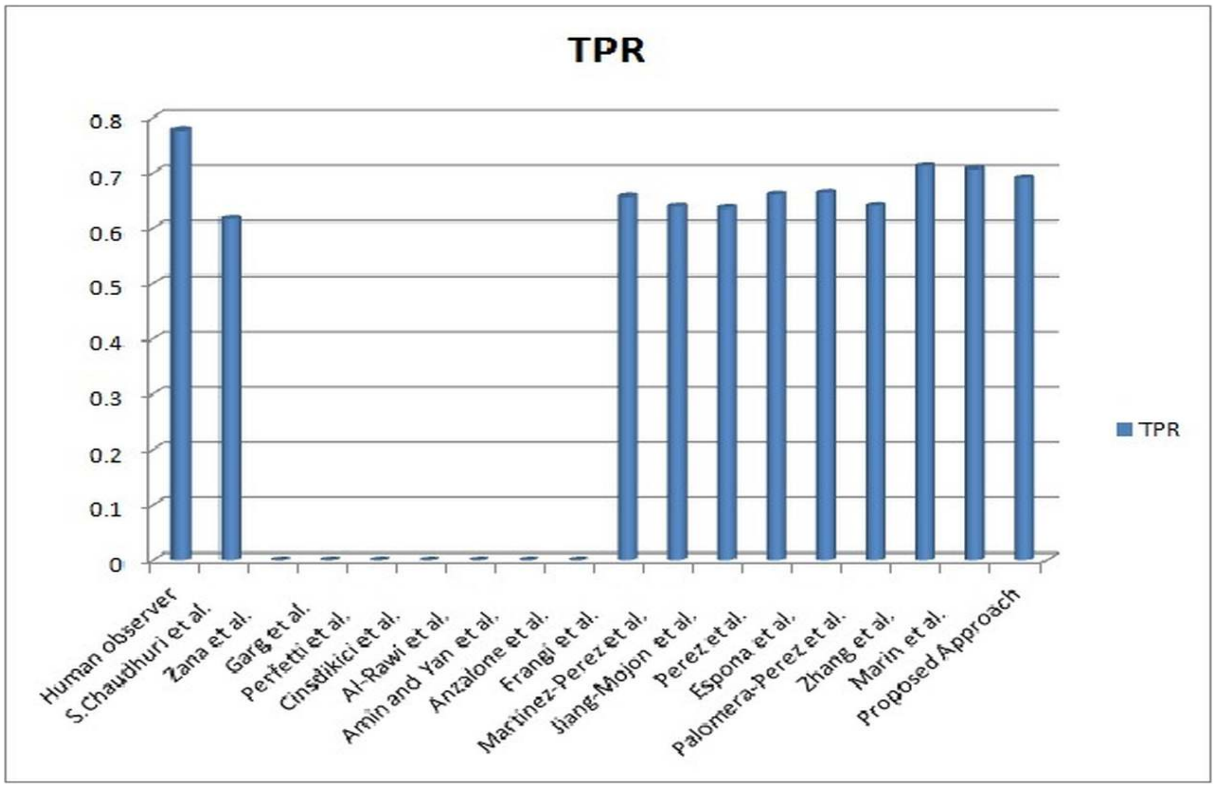

(a)

Figure 3.8: Comparison of TPR for DRIVE database.

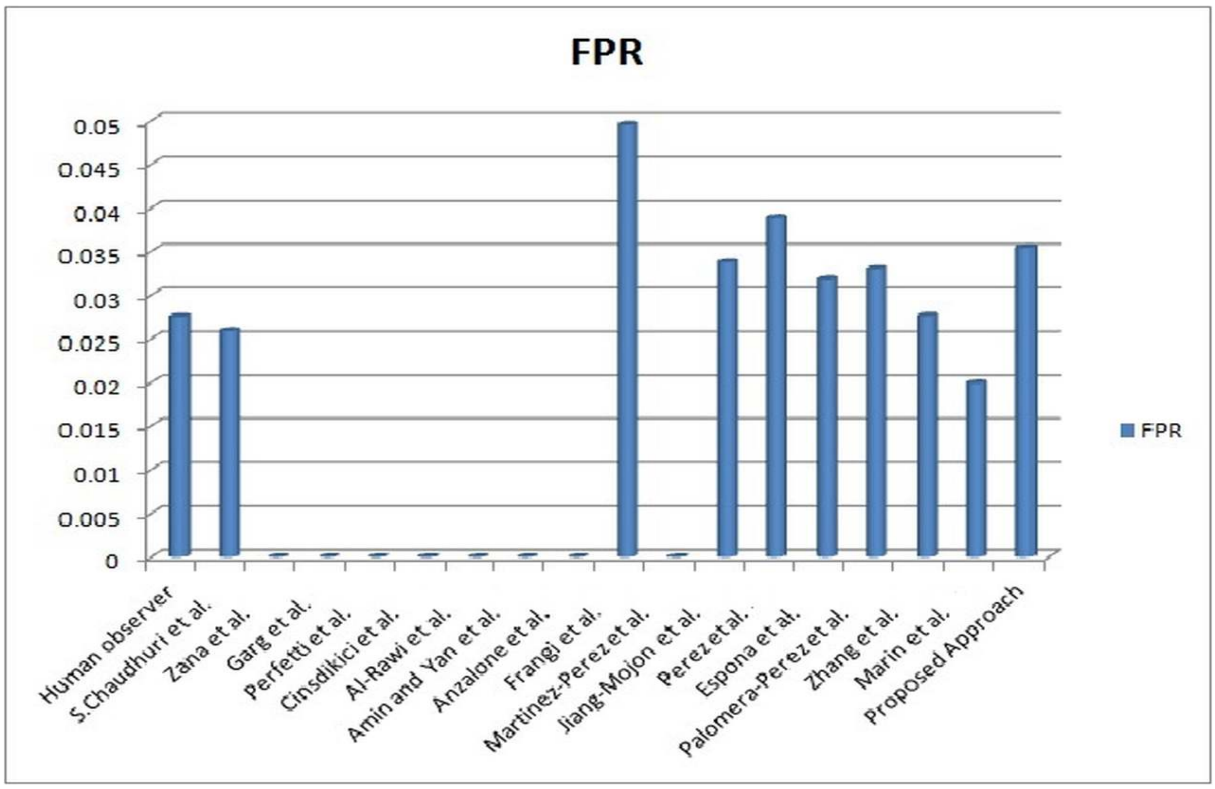

(a)

Figure 3.9: Comparison of FPR for DRIVE database.

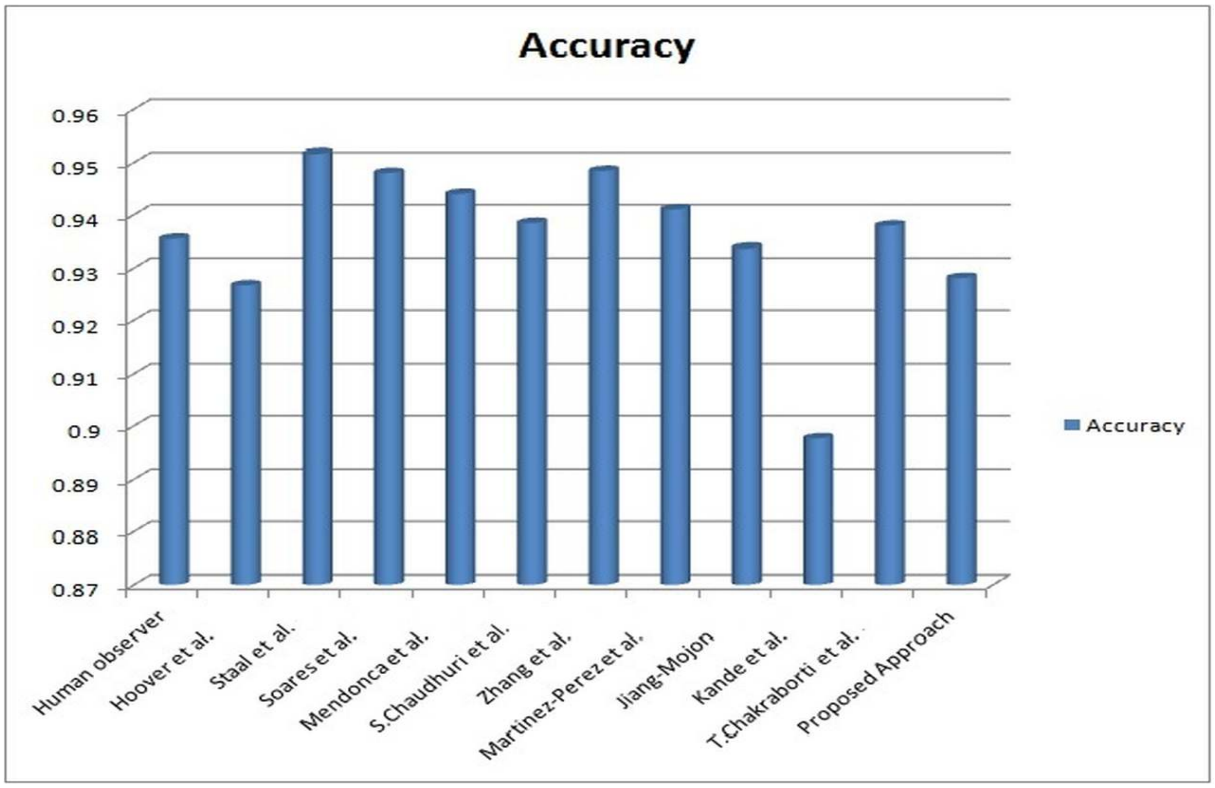

(a)

Figure 3.10: Comparison of Accuracy for STARE database.

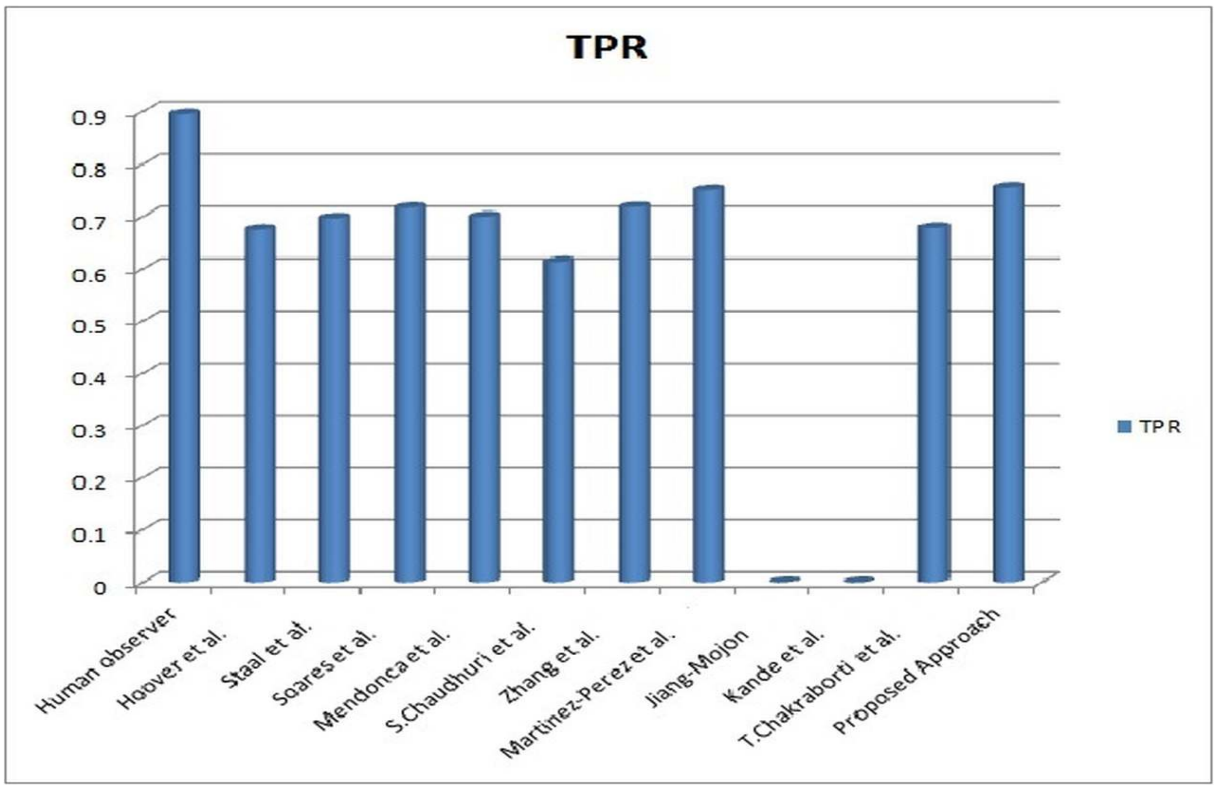

(a)

Figure 3.11: Comparison of TPR for STARE database.

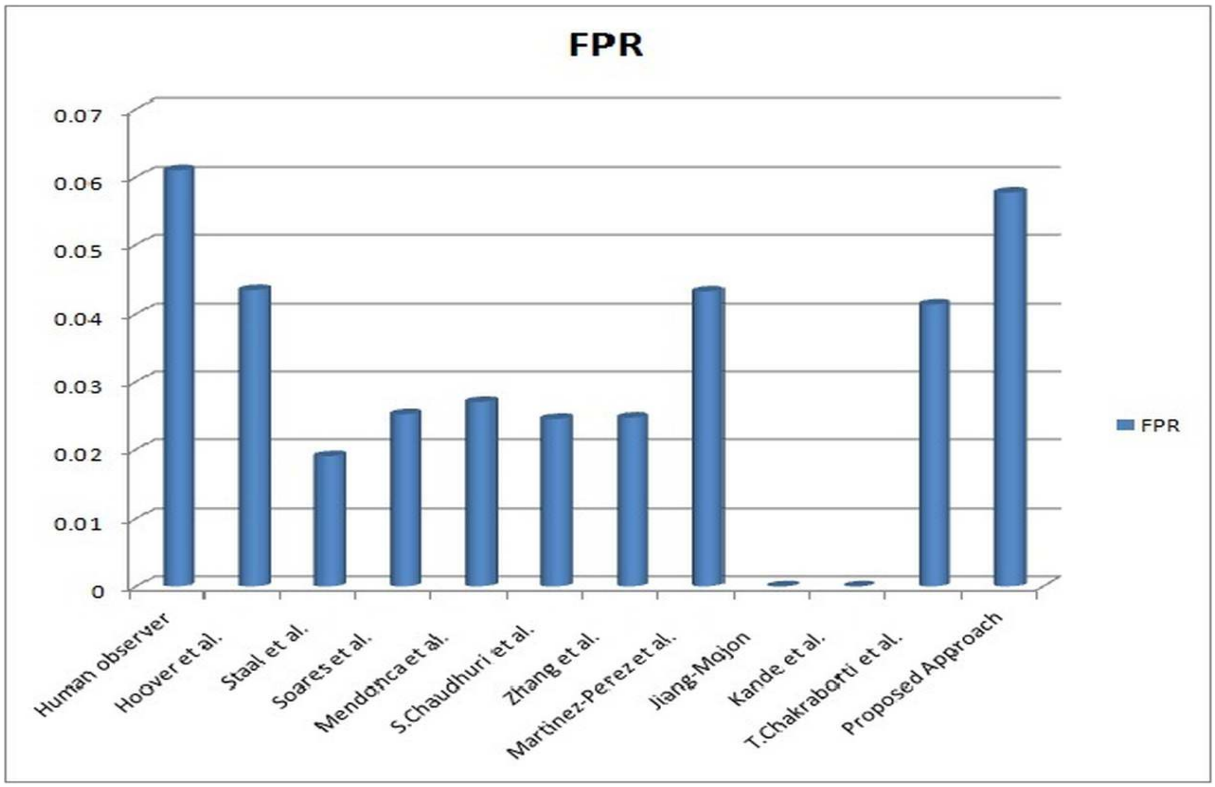

(a)

Figure 3.12: Comparison of FPR for STARE database.

Table 3.2: Comparison of Vessel segmentation results on the STARE database

Author's name	**TPR**	**FPR**	**Accuracy**
Human observer	0.8949	0.061	0.9354
Hoover *et al.* [2]	0.6751	0.0433	0.9267
Staal *et al.* [26]	0.697	0.019	0.9516
Soares *et al.* [48]	0.7165	0.0252	0.948
Mendonca *et al.* [56]	0.6996	0.027	0.944
Chaudhuri *et al.* [12]	0.6134	0.0245	0.9384
Zhang *et al.* [47]	0.7177	0.0247	0.9484
Martinez-Perez *et al.* [65]	0.7506	0.0431	0.9410
Jiang *et al.* [44]	—	—	0.9337
Kande *et al.* [54]	—	—	0.8976
Chakraborti *et al.* [148]	0.6786	0.0414	0.9379
Proposed Approach (SDOG-MF)	**0.7553**	**0.0577**	**0.9281**

The comparative analysis of proposed SDOG-MF approach on the STARE database is presented in Table 3.2 and graphical representation of comparative performances are also shown in Figure 3.10, Figure 3.11, and Figure 3.12. The proposed approach has been implemented on 20 retinal images, that contains 11 normal and 9 pathological retinal

images and we used the manually segmented ground truth image by first observer for evaluating the performance measures. The performance measures of retinal blood vessel segmentation methods proposed by Hoover *et al.* [2] and Soares *et al.* [48] were evaluated from their websites. The performance of the approach proposed by Staal *et al.* [26], Mendonca *et al.* [56], Kande *et al.* [54] and Chakraborti *et al.* [148] were obtained from their original papers. The TPR and FPR measures of our proposed SDOG-MF approach are better for STARE database than the various existing approaches and overall accuracy is slightly inferior to some other existing approaches as shown in Table 3.2 and the graphical representation of TPR, FPR, and Accuracy are given in Figure 3.10, Figure 3.11, and Figure 3.12 respectively..

3.5 Conclusions

The retinal blood vessels are highly responsible for the detection of retinal pathology hence extraction of retinal blood vessels from their background is a prominent task. Therefore this chapter presented a novel extension of matched filter based retinal blood-vessel segmentation approach, namely SDOG-MF. The SDOG-MF approach was based on second-order derivative of the Gaussian (SDOG) and local entropy thresholding. The proposed approach was able to identify thin retinal blood vessels as well as thick blood vessels. The proposed method has been implemented on twenty retinal images taken from a test set of DRIVE database and nineteen out of twenty retinal images taken from STARE database. The segmented results of the DRIVE and STARE database were compared with hand-labeled ground truth images available in the respective database. The performance of the proposed algorithm was compared with some other existing standard methods for the same task available in the literature and it was found that the accuracy of proposed approach was good enough for retinal fundus images taken from a test set of DRIVE database whereas the TPR and FPR was improved in case of retinal fundus images taken from STARE database.